ARTICLES

Journal of Semiconductors
(2021) 42, 122001
doi: 10.1088/1674-4926/42/12/122001

Quantum transport simulation of the two-dimensional GaSb transistors

Panpan Wang, Songxuan Han, and Ruge Quhe†

State Key Laboratory of Information Photonics and Optical Communications and School of Science, Beijing University of Posts and Telecommunications, Beijing 100876, China

Abstract: Owing to the high carrier mobility, two-dimensional (2D) gallium antimonite (GaSb) is a promising channel material for field-effect transistors (FETs) in the post-silicon era. We investigated the ballistic performance of the 2D GaSb metal–oxide–semiconductor FETs with a 10 nm-gate-length by the ab initio quantum transport simulation. Because of the wider bandgap and better gate-control ability, the performance of the 10-nm monolayer (ML) GaSb FETs is generally superior to the bilayer counterparts, including the three-to-four orders of magnitude larger on-current. Via hydrogenation, the delay-time and power consumption can be further enhanced with magnitude up to 35% and 57%, respectively, thanks to the expanded bandgap. The 10-nm ML GaSb FETs can almost meet the International Technology Roadmap for Semiconductors (ITRS) for high-performance demands in terms of the on-state current, intrinsic delay time, and power-delay product.

Key words: 2D GaSb; 10 nm MOSFET; hydrogenation; density functional theory; quantum transport simulation

Citation: P P Wang, S X Han, and R G Quhe, Quantum transport simulation of the two-dimensional GaSb transistors[J]. *J. Semicond.*, 2021, 42(12), 122001. http://doi.org/10.1088/1674-4926/42/12/122001

1. Introduction

In the past few decades, the development of Si-based microelectronics obeys the performance scaling trend predicted by Moore's law. As the building block of the microelectronics, silicon metal–oxide–semiconductor field-effect transistors (MOSFETs) behave as switches and are integrated into logic circuits to realize logic operations. Nowadays, the continuous and aggressive scaling of MOSFETs has highly increased the capability of calculation. However, traditional Si MOSFET scaling could no longer satisfy the original trend as the power density dissipated by logic chips got about 100 W/cm^2[1]. Such a phenomenon originates from the so-called "short channel effects". In the ultra-short Si MOSFET, it becomes very hard to suppress the source to drain leakage by gating.

A direct way to enhance the gate electrostatics is by decreasing the thickness of the semiconducting channel. The nature length scale λ is defined as $\lambda = \sqrt{\frac{t_{ch}t_{ox}\varepsilon_{ch}}{\varepsilon_{ox}}}$ [2]. t_{ch}, ε_{ch}, t_{ox} and ε_{ox} are the thickness and dielectric constant of the channel and dielectric oxide layer, respectively. λ stands for the distance across which the electric field can penetrate from the electrode region to the device's channel region. A smaller λ implies better gate controllability. Obviously, a thin channel thickness t_{ch} enhances the gate control ability and suppresses the short channel effects. Tremendous efforts have been made in the fabrication of the ultrathin-body silicon FETs[3]. Although the thickness of Si bulk can be reduced even to 1 nm, non-ideal scattering of charge carriers happens due to thickness variation and surface dangling bonds[4–6]. The phenomenon leads to enormous degradation of carrier mobility compared with the bulk Si. Two-dimension (2D) semiconductors have attracted intense interest for their atomically thin body thickness, featuring a dangling-bond-free surface and little mobility variation[7–11]. While the instability and zero-gap semimetallic character in the 2D form of Si (silicene)[12] hinder its application, seeking 2D analogs of other semiconductors is a possible solution.

Most III–V semiconductors have smaller effective masses than Si, and thus higher drift velocity[13–16], which endows them great potential in high-speed MOSFET. Gallium-based materials possess high carrier mobility, which is advantageous for MOSFETs. Moreover, in the 2D region, research shows that the effective mass of monolayer (ML) GaSb is smaller than ML GaN, GaP, and GaAs, implying high carrier mobility of ML GaSb[17]. Thus, the ultrathin GaSb is of high interest for the post-silicon electronic.

In this paper, we investigate 10 nm double-gated (DG) n- and p-type metal–oxide–semiconductor FETs with ML and bilayer (BL) GaSb by using ab initio quantum transport simulations. The DG ML GaSb MOSFETs show on-currents (I_{on}) ranging from 1.0×10^1 to 1.3×10^3 μA/μm. Good gate electrostatics with the subthreshold swing ranging from 87 and 120 mV/dec and transconductance from 7.9×10^3 to 2.8×10^4 μS/μm are observed. The power-delay products (PDP) and delay time (τ) of almost all the studied ML GaSb MOSFETs are lower than the requirements of ITRS and IRDS, which indicates their competitiveness in low-power applications.

2. Model and method

The two-probe 10 nm-gate-length DG MOSFET is constructed with intrinsic ML and BL GaSb and their hydrogenated counterparts as the channel, respectively. The source and drain are highly doped 2D GaSb. The doping concentration is

Correspondence to: R G Quhe, quheruge@bupt.edu.cn
Received 27 APRIL 2021; Revised 29 MAY 2021.

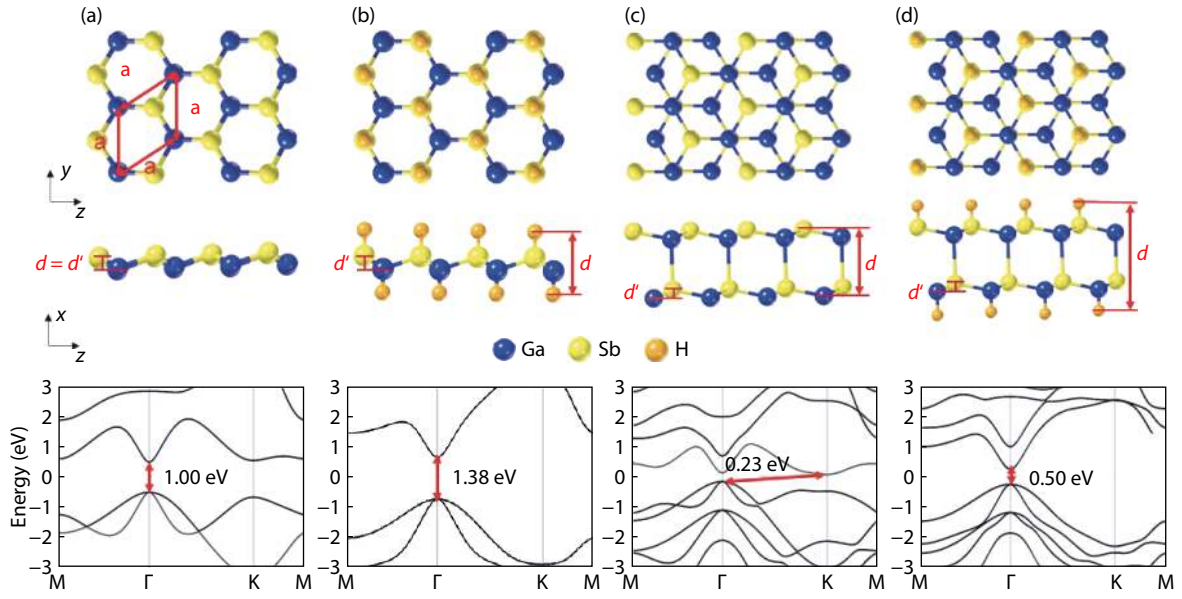

Fig. 1. (Color online) Top and side views and band structures of (a) ML GaSb, (b) ML h-GaSb, (c) BL GaSb, and (d) BL h-GaSb.

5×10^{13} cm^{-2}[18]. We adopt SiO_2 dielectric with 3.9 dielectric constant and 0.56 nm equivalent oxide thickness (EOT). The supply voltage (V_{dd}) is set to 0.45 V (= V_b) in terms of the ITRS standard.

We apply the density functional theory (DFT) combined with the nonequilibrium Green's function (NEGF) formalism in the Atomistix ToolKit package to calculate the electronic and transport properties[19, 20]. The following Landauer–Büttiker formula gives the drain current I_{ds}:

$$I_d(V_b, V_g) = \frac{2e}{h}\int_{-\infty}^{+\infty}\{T(E, V_b, V_g)[f_S(E-\mu_S)-f_D(E-\mu_D)]\}dE, \quad (1)$$

where e is the elementary charge, h is the Planck constant, $T(E, V_b, V_g)$ is the probability of transmission at a given gate voltage V_g and voltage V_b, f_S and f_D are the Fermi–Dirac distribution function for the source and drain, respectively, and μ_S and μ_D are the electrochemical potentials of the source and drain, respectively. OpenMX basis set with a mesh cut-off energy of 200 hatree was used. The temperature was set to 300 K. The Brillouin zone was sampled with separations of 0.01 Å^{-1}[21]. We applied the Neumann boundary condition along the direction out of the GaSb plane, the Dirichlet boundary condition along the transport direction, and the periodic boundary condition along the transverse direction of the transistors. The generalized gradient approximation (GGA) in the form of Perdew–Burke–Ernzerhof (PBE) potential was used to describe the exchange-correlation interaction in the transistor[22].

3. Results and discussion

We investigate four types of GaSb-based materials: ML GaSb, BL GaSb, and their hydrogenated counterparts. The hydrogenated GaSb is noted as h-GaSb for short. These structures are shown in Fig. 1, and the optimized parameters are listed in Table 1. ML GaSb is a buckled honeycomb structure with an optimized lattice parameter of 4.36 Å and thickness of 0.80 Å. After hydrogenation, the lattice parameter of ML GaSb is slightly increased to 4.37 Å and thickness is increased to 2.19 Å. The increment of the thickness comes not only from the introduction of the H atoms, but also from the deformation of the Ga–Sb bonds. d' is defined by the distance between two Ga and Sb atomic planes. The full hydrogenation makes Sb atom rise and Ga atom lower, increasing d' of ML GaSb from 0.81 to 0.87 Å. It is consistent with previous theoretical studies on the ML III–V compounds[15]. BL GaSb is truncated from the zinc-blende bulk structure. The lattice parameters of BL GaSb and h-GaSb are close to their ML counterparts, and the thicknesses are 4.46 and 7.69 Å, respectively. A similar increase of d' from 0.81 to 0.90 Å is observed in the BL after hydrogenation.

Table 1. Structural and electronic parameters of monolayer (ML) and bilayer (BL) GaSb. h-GaSb stands for the hydrogenated layer.

Parameter	ML GaSb	ML h-GaSb	BL GaSb	BL h-GaSb
a (Å)	4.36	4.37	4.38	4.37
d (Å)	0.81	2.19	4.46	7.69
d' (Å)	0.81	0.87	0.81	0.90
Δ (eV)	1.00	1.38	0.23	0.50
m_e^* (m_0)	0.070	0.081	0.588	0.086
m_h^* (m_0)	0.485	0.620	0.685	0.555

a: lattice parameter; d: thickness; d': the distance between Ga and Sb atom along the direction out of the plane; Δ: bandgap; m_e^*: the electron effective mass; m_h^*: the heavy-hole effective mass. m_0: the free effective mass.

Freestanding ML GaSb may has dangling bonds on its surface, this feature might affect the stability of the material. While there is no dangling bond on ML h-GaSb, since the surface is passivated. Comparing the phonon spectra of ML GaSb[23] and ML MoS_2[24], ML GaSb may not be as dynamically stable as the latter one. However, the previous studies have shown that the formation energy of ML GaSb[23] is lower than that of ML SiC[25], which had been successfully manufactured, so it is possible to synthesis ML GaSb. In addition, selecting lattice-matched high atomic density surfaces of substrates enhances the stability of ML GaSb. A suitable substrate like Pd can energetically stabilize materials during the growth process[26].

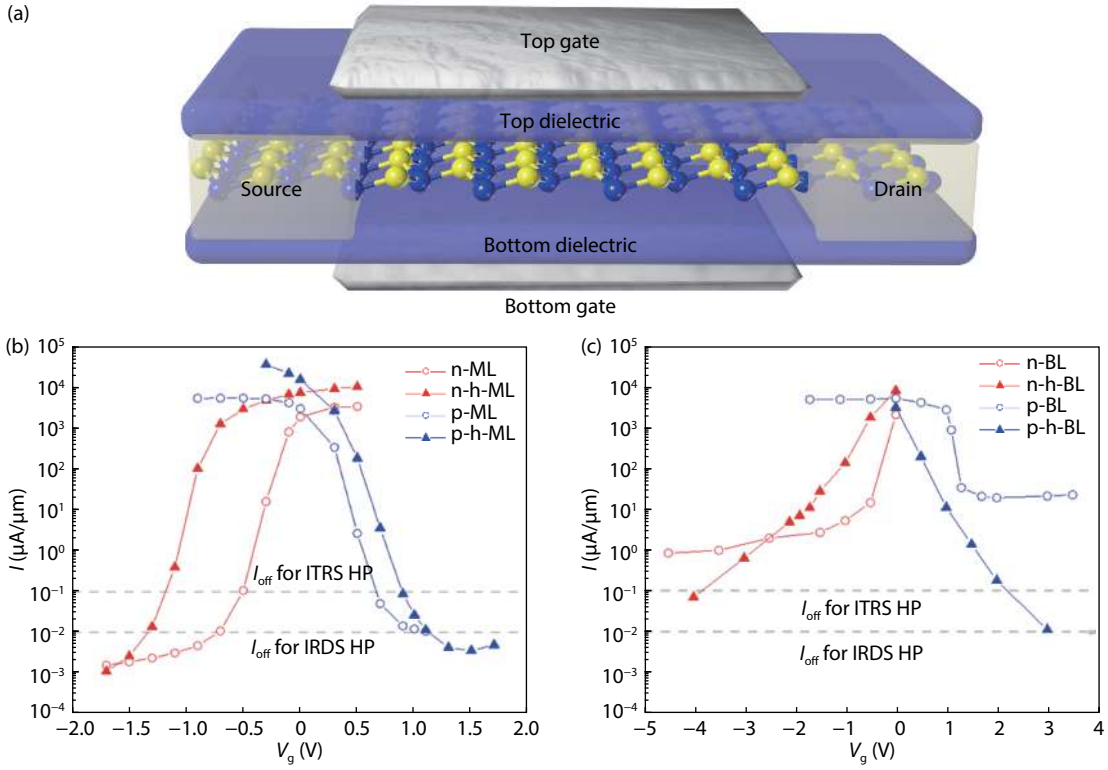

Fig. 2. (Color online) (a) Schematic model of DG ML GaSb MOSFET with 10 nm gate length. (b, c) Transfer characteristic of ML GaSb and h-GaSb and BL GaSb and h-GaSb.

The electronic band structures of 2D GaSb and h-GaSb along the high symmetric k-path M–Γ–K–M are shown in Fig. 1. ML GaSb is a semiconductor with a direct bandgap of 1.00 eV. The valence band maximum (VBM) and conduction band minimum (CBM) are located at Γ point. After hydrogenating, the crystal remains a direct bandgap at Γ point with an expended size of 1.38 eV. Compared with the ML ones, the bandgaps of the BL counterparts are much smaller. BL GaSb shows an indirect bandgap of 0.23 eV with VBM located at Γ point and CBM at K point. BL h-GaSb shows a direct bandgap of 0.5 eV at Γ point. A bandgap of at least 0.4 eV is required for the semiconductor as the channel in the transistor[27] so as to achieve an on/off current ratio large enough for practical use. ML GaSb, ML h-GaSb and BL h-GaSb are promising in this regard.

The effective mass (m^*) is estimated from the band structure, in accordance with the equation: $m^* = \left(\frac{1}{\hbar^2}\frac{d^2E}{dk^2}\right)^{-1}$. We select the heavy-hole band to calculate hole effective mass here. The effective masses of ML GaSb and h-GaSb range from $0.070m_0$ to $0.685m_0$. The electron effective masses except for BL GaSb's, under $0.10m_0$, are much less than bulk Si ($0.273m_0$ to $0.367m_0$)[28]. It is noted that the values of the electron and hole effective mass of the BL GaSb are closed. While for the other three materials, the heavy-hole effective masses are generally about seven times as large as the electron counterparts. Therefore, a relatively better n-type performance of the devices based on the ML GaSb, h-GaSb and BL h-GaSb are expected than p-type ones.

The transfer characteristics of the 2D GaSb MOSFET are shown in Figs. 2(b) and 2(c). The current of p-type devices decreases as the gate voltage increases, and the n-type ones are in contrast, which corresponds with the general trend that devices switch between the off-state and on-state. Additionally, comparing the transfer curves of the n- and p-type devices based on the same material, the ML GaSb MOSFETs have the most symmetrical current trend. The off-current (I_{off}) is set to 0.1 and 0.01 μA/μm in terms of the high-performance (HP) requirement of 2015 ITRS and 2020 IRDS, respectively. From the pictures, all the devices with ML materials can meet the two requirements for I_{off}, except for the BL GaSb n- and p-MOSFETs. The lowest current of BL GaSb MOSFET in the considered voltage range (–4.5 to 3.5 V) is about one or two orders of magnitude larger than 0.1 μA/μm I_{off}. i.e., the BL GaSb MOSFETs are hard to turn "off". This phenomenon is related to the small bandgap of 0.23 eV in BL GaSb. Thus, hydrogenation of the BL GaSb is suggested in order to increase the bandgap and thus suppress the source to drain leakage so that to meet the off-current requirement.

With I_{off} = 0.1 μA/μm selected from the HP requirement of ITRS 2015 edition for 2027 horizons, I_{on} can be determined by the supply voltage V_{dd} (0.45 V): $|V_{g,on} - V_{g,off}| = V_{dd}$. Besides, from the HP standard of IRDS 2020 edition for 2028 horizons, we also calculated the I_{on} with 0.01 μA/μm I_{off} and 0.65 V V_{dd}. A higher I_{on} indicates a faster logic transition speed of the switch. All I_{on} of ML GaSb and h-GaSb MOSFETs ranges from 1.0×10^1 to 1.3×10^3 μA/μm. In comparison, I_{on} of BL ones is lower than 1 μA/μm, which are apparently lower than most ML ones. In Fig. 3(a), we plot the on-current as a function of the effective mass in the 2D semiconductor that we considered except BL GaSb (because the simulated lowest current of the 10 nm BL GaSb MOSFET is larger than the I_{off} requirement of 0.1 μA/μm). The n-MOSFETs behave better than the p-type counterparts in terms of the on-current mainly because of the much lighter effective mass. Consider-

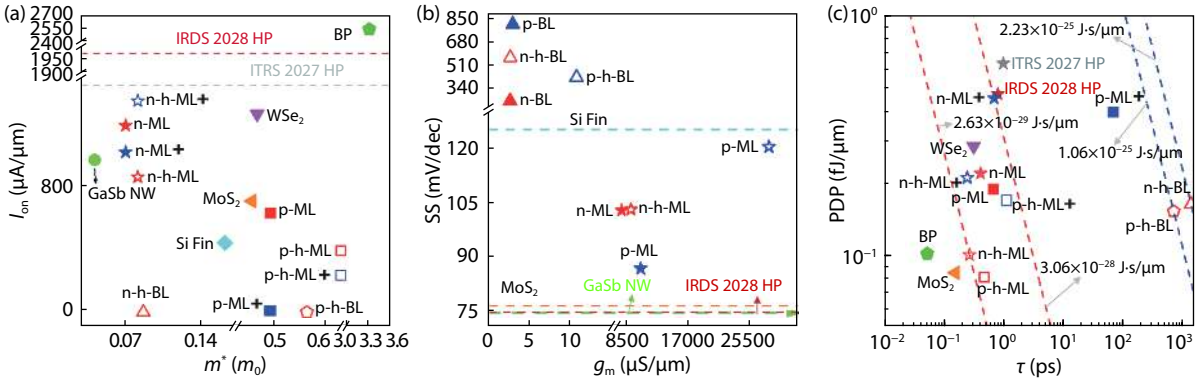

Fig. 3. (Color online) (a) On-current versus the effective mass m^*, (b) subthreshold swing versus transconductance, and (c) power-delay products versus delay time. Labels with and without cross-shaped subscripts represent the values calculated according to IRDS and ITRS standards, respectively. The data of other transistors with a similar gate length are also included for comparison: GaSb p-nanowire[29], BP (transfer along zigzag direction)[30], WSe_2[31], MoS_2 MOSFETs[9], and Si FinFET[32].

ing materials of electron-effective masses (< $0.087m_0$), I_{on} shows an increasing trend with decreasing m^* for GaSb. When heavy-hole effective masses of GaSb are relatively higher (> $0.48m_0$), there is no obvious dependence between I_{on} and effective mass. This phenomenon originates from the competition between the factors of mobility and gate controllability. While a small effective mass is beneficial for higher mobility, a larger effective mass implies a larger density of state near the Fermi level and thus better gate controllability. The latter factor becomes especially important in the ultrashort MOSFETs. As a result, no simple linear relation between the effective mass and the on-current is found. It is noted that for ML GaSb MOSFETs (no matter n- or p-type), the hydrogenation enhances the I_{on} of IRDS set, but ITRS ones are opposite. This may result from different slopes of transfer curves at different gate voltage range.

It is intriguing to benchmark the performance of ML GaSb MOSFETs against transistors with other channel materials. Almost both the ML GaSb and h-GaSb MOSFETs show higher I_{on} than Si FinFET with a similar size of 10 nm. Compared with the 10 nm MOSFETs based on other commonly studied 2D materials like WSe_2 and MoS_2[31, 33], the ML GaSb and h-GaSb MOSFETs are not inferior in I_{on}. With the 2015 ITRS HP settings, I_{on} of ML GaSb MOSFETs can fulfill 33%–83% requirement. The latest IRDS requires a lower off-current (0.01 μA/μm) and a higher on-current (2.0×10^3 μA/μm) for the HP application in 2028. With this off-current, the gap of I_{on} between n- and p-type MOSFETs further extends. I_{on} of devices with ML materials can meet 52%–69%, and p-type counterparts only satisfy 1%–11% of the IRDS standard. To further increase I_{on} of GaSb-based MOSFETs, we can manipulate the electronic structure by introducing a compressive biaxial strain. Research indicates that with a 2.0% biaxial compressive strain, the maximum hole mobility of GaSb p-MOSFETs has increased 2.86 times, compared with the freestanding one[4, 34–36].

The electronic control ability of the MOSFET gate is highly significant. The subthreshold swing (SS) and transconductance (g_m) evaluate the control ability in different regions. SS is a parameter describing the gate control ability at the subthreshold area. It is defined as $SS = \frac{\partial V_g}{\partial \lg I_D}$, revealing the gate voltage needed to change the drain–source current by one decade. Transconductance indicates the characteristic of the gate control ability at the superthreshold region, and is calculated by $g_m = \frac{\partial I_d}{\partial V_g}$. As shown in Fig. 3(b), ML GaSb and h-GaSb MOSFETs show relatively small SS (87 to 120 mV/dec) and large g_m (7.9×10^3 to 2.8×10^4 μS/μm). On the other hand, SS of BL GaSb and h-GaSb ones are higher than 200 mV/dec, and g_m is lower than 12 μS/μm. The reason lies in the increased thickness of BL GaSb and thus reduced coupling of the top and bottom gate, which brings a weaker electric field. Additionally, we can see that hydrogenation cannot enhance the performance of SS for both the ML BL GaSb MOSFETs (Fig. 3(b)). Comparing the gate control abilities of GaSb MOSFETs with other transistors, SS of ML GaSb MOSFETs are higher than Si FinFET[32], and lower than 2D MoS_2 MOSFET[29]. While the innovation of the device mechanism is needed to overcome the Boltzmann limit of 60 mV/dec[37] and thus the ITRS requirement (25 mV/dec), the lowest SS in the studied 2D GaSb MOSFETs is already very close to the IRDS requirement (75 mV/dec).

To understand the mechanism of gate control of MOSFETs, we calculate the local density of state for n-type DG MOSFETs with ML GaSb, ML h-GaSb, and BL h-GaSb. We define a maximum hole barrier height Φ_B as the energy barrier between the highest energy level of the channel VBM and the source Fermi energy level. In Figs. 4(a)–4(c), Φ_B of DG ML freestanding GaSb MOSFET is 0.78 eV when V_g = –0.9 eV at the off-state. It hinders the carrier transport from source to drain, and the current is mainly contributed by the tunneling current I_{tunnel}. With the increase of gate voltage (–0.3 eV), the device turns to the intermediate state, and Φ_B decreases to 0.32 eV. Both the tunneling current I_{tunnel} and the thermionic current I_{therm} contribute significantly to the total current of 16 μA/μm. They are separated by the top of barrier height. When enhancing gate voltage to 0.3 eV, the barrier disappears, and I_{on} reaches 3.4×10^3 μA/μm with I_{therm}'s main contribution.

Compared with the ML GaSb MOSFET, the ML h-GaSb MOSFET's gate modulation (Figs. 4(d)–4(f)) is similar on the overall trend, but Φ_B becomes larger in every state. From the off-state (V_g = –1.3 eV) to the intermediate-state (V_g = –0.9 eV) to the off-state (V_g = 0.3 eV), Φ_B decreases from 1.69 to 0.9 and to 0 eV, and the current increases from 0.01

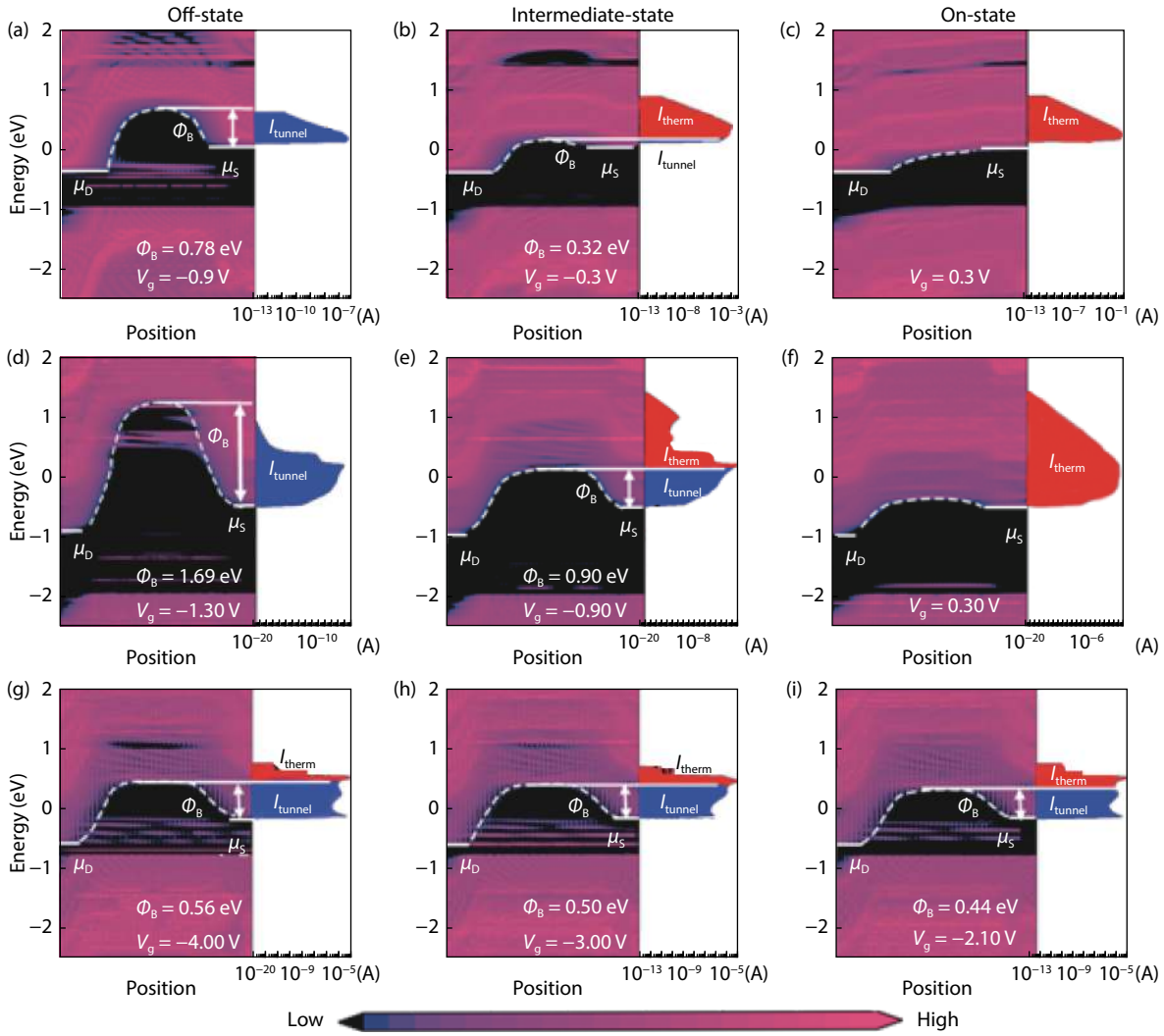

Fig. 4. (Color online) Position resolved local density of state and spectral current in the channel region of (a–c) ML GaSb, (d–f) ML h-GaSb and (g–i) BL h-GaSb at different states. μ_s and μ_d are the electrochemical potential of the source and drain, respectively. Φ_B is the effective barrier height.

to 106 and to 9528 μA/μm. However, during the on-off state transition, the BL h-GaSb MOSFET (Figs. 4(g)–4(i)) performs slightly differently. Its Φ_B decreases much smaller than the ML material MOSFET one. In the meantime, the current increases much smaller from 0.07 (off-state) to 0.6 (intermediate-state) and to 4.9 μA/μm (on-state). It depicts the worst control ability and the lowest switch speed among three MOSFETs.

Next, we consider the delay time (τ) and power consumption. The delay time of the transistor straightly indicates the switching speed, which can be calculated by $\tau = \frac{C_{total}V_{dd}}{I_{on}}$. C_{total} is defined as the total capacitance, including gate capacitance (C_g) and fringing capacitance (C_f). C_g can be calculated by $C_g = \frac{\partial Q_{ch}}{\partial V_g}$, where Q_{ch} is the total charge of the central region. The ratio $\frac{C_f}{C_g}$ is calculated to be around 1 to 2 for the 10 nm MOSFETs[38–40], and here we set $\frac{C_f}{C_g}$ to 2. In order to evaluate the performance more intuitionally, we also extracted the energy-delay product (EDP = PDP × τ), which can measure power dissipation and transition speed simultaneously. Except for ML GaSb p-MOSFET under IRDS settings, the EDP values of the ML GaSb and h-GaSb MOSFETs are in the range similar to those of MoS_2 and WSe_2, while those of the BL GaSb and h-GaSb ones are far larger than them. As presented in Fig. 3(c), almost all the EDP of ML GaSb MOSFETs (from 2.6 × 10^{-29} to 3.1 × 10^{-28} J·s/μm) satisfy the ITRS and IRDS standards, while BL ones (from 1.1 × 10^{-25} to 2.2 × 10^{-25} J·s/μm) have larger EDP than the standard and only meet the PDP requirement. ML and BL MOSFETs are similar in the power consumption but differ a lot in the delay time, which may result from the latter ones' extremely smaller on-current than former ones. All the considered ML materials own lower PDP than 0.45 fJ/μm and shorter delay time than 1.10 ps. The smallest EDP belongs to ML h-GaSb n-MOSFET (ITRS settings). Hydrogenation boosts the switching speed of ML GaSb MOSFET, and reduces the PDP to lower than half of the freestanding counterpart, bringing on the smallest EDP. The main cause is found to be the decreased C_{total}.

As for radio-frequency (RF) devices, one of the most important figures of merit is the cut-off frequency (f_t). The cut-off frequency is the upper frequency at which the magnitude of the current gain has dropped to unity (0 dB), meaning the transistor loses the amplified ability. We can calculate f_t using the equation: $f_t = \frac{g_m}{2\pi C_{total}}$. Here, f_t is influenced by the transconductance g_m and the total gate capacitance C_{total}. BL GaSb only has f_t at about GHz, while ML GaSb's can

reach THz. Freestanding ML GaSb n- and p-MOSFET are 1.2 and 1.8 THz, respectively. f_t of the ML GaSb MOSFETs are larger than those of graphene-based FETs (0.3 THz) and silicane MOSFETs (0.5 THz) at room temperature[41], but still need the effort to reach the level of 2D MoS_2 (4 THz) and 2D WSe_2 (5 THz)[42]. Luckily, hydrogenation enhances the cut-off frequency to 2.9 THz for the ML h-GaSb n-MOSFET and 11 THz for the ML h-GaSb p-MOSFET. In particular, this cut-off frequency of 11 THz in the ML h-GaSb p-MOSFET is superior among all the MOSFETs mentioned above. Thus, ML h-GaSb is highly suggested to be tested for the RF devices.

In our simulation, SiO_2 of 0.56 nm thick is used as the dielectrics. Such a thin dielectric will result in a high gate tunneling leakage current in practice. The high gate leakage will lower the circuit performance severely, and it is a critical issue especially in the sub-nanometer scale. Changing SiO_2 into other high-k dielectrics such as TiO_2 and HfO_2 can overcome this disadvantage[43]. High-k materials have larger capacitance equivalent thickness than SiO_2, and thus a better ability to suppress the leakage.

4. Conclusion

Inspired by the high mobility of III–V binary materials, we simulated the 2D GaSb n- and p-MOSFETs with a gate length of 10 nm based on ab initio quantum transport simulations. BL GaSb MOSFETs perform significantly worse than the ML ones, owing to their relatively smaller bandgap and heavier masses. Additionally, it is found that power-delay products and delay time can be best improved by about 35% and 57%, respectively, with full hydrogenation. The on-currents of ML GaSb MOSFETs range from 1×10^1 to 1.3×10^3 μA/μm, and the SS cover from 87 to 120 mV/dec. ML GaSb transistors show a fast delay time of 0.24 to 1.10 ps and low power-delay products of 0.08 to 0.45 fJ/μm. In general, the ML GaSb and h-GaSb MOSFETs perform similarly to the commonly studied ML MoS_2 and WSe_2 counterparts with the same gate length of 10 nm, in terms of a few figures of metrics including the on-current, PDP, and delay time. Therefore, making GaSb thinner, ideally fabricating the thinnest ML GaSb, is worthy of being tested for the ultrashort transistors in the experiment.

Acknowledgements

This work was supported by the National Natural Science Foundation of China (No. 91964101), the Fund of State Key Laboratory of Information Photonics and Optical Communications (Beijing University of Posts and Telecommunications) and the Research Innovation Fund for College Students of Beijing University of Posts and Telecommunications.

References

[1] Frank D J. Power-constrained CMOS scaling limits. IBM J Res Dev, 2002, 46, 235
[2] Yan R H, Ourmazd A, Lee K F. Scaling the Si MOSFET: From bulk to SOI to bulk. IEEE Trans Electron Devices, 1992, 39, 1704
[3] Hu C. FinFET and UTB: How to make very short channel MOSFETs. ECS Trans, 2013, 50, 17
[4] Uchida K, Koga J, Takagi S I. Experimental study on carrier transport mechanisms in double-and single-gate ultrathin-body mosfets. IEEE International Electron Devices Meeting, 2003, 33.5.1
[5] Uchida K, Watanabe H, Kinoshita A, et al. Experimental study on carrier transport mechanism in ultrathin-body SOI nand p-MOSFETs with SOI thickness less than 5 nm. Dig Int Electron Devices Meet, 2002, 47
[6] Uchida K, Watanabe H, Koga J, et al. Experimental study on carrier transport mechanism in ultrathin-body SOI MOSFETs. International Conference on Simulation of Semiconductor Processes and Devices, 2003, 8
[7] Bandurin D A, Tyurnina A V, Yu G L, et al. High electron mobility, quantum Hall effect and anomalous optical response in atomically thin InSe. Nat Nanotechnol, 2017, 12, 223
[8] Li L K, Yu Y J, Ye G, et al. Black phosphorus field-effect transistors. Nat Nanotechnol, 2014, 9, 372
[9] Radisavljevic B, Radenovic A, Brivio J, et al. Single-layer MoS_2 transistors. Nat Nanotechnol, 2011, 6, 147
[10] Schwierz F, Pezoldt J, Granzner R. Two-dimensional materials and their prospects in transistor electronics. Nanoscale, 2015, 7, 8261
[11] Tao L, Cinquanta E, Chiappe D, et al. Silicene field-effect transistors operating at room temperature. Nat Nanotechnol, 2015, 10, 227
[12] Acun A, Poelsema B, Zandvliet H J W, et al. The instability of silicene on Ag(111). Appl Phys Lett, 2013, 103, 263119
[13] Doornbos G, Passlack M. Benchmarking of III–V n-MOSFET maturity and feasibility for future CMOS. IEEE Electron Device Lett, 2010, 31, 1110
[14] del Alamo J A, Antoniadis D A, Lin J Q, et al. Nanometer-scale III-V MOSFETs. IEEE J Electron Devices Soc, 2016, 4, 205
[15] Lü X, He S S, Lian H X, et al. Structural, electronic, and optical properties of pristine and bilayers of hexagonal III-V binary compounds and their hydrogenated counterparts. Appl Surf Sci, 2020, 531, 147262
[16] Riel H, Wernersson L E, Hong M, et al. III-V compound semiconductor transistors — from planar to nanowire structures. MRS Bull, 2014, 39, 668
[17] Bahuguna B P, Saini L K, Sharma R O, et al. Strain and electric field induced metallization in the GaX (X = N, P, As & Sb) monolayer. Physica E, 2018, 99, 236
[18] Low T, Rodin A S, Carvalho A, et al. Tunable optical properties of multilayer black phosphorus thin films. Phys Rev B, 2014, 90, 075434
[19] Brandbyge M, Mozos J L, Ordejón P, et al. Density-functional method for nonequilibrium electron transport. Phys Rev B, 2002, 65, 165401
[20] Soler J M, Artacho E, Gale J D, et al. The SIESTA method for ab initio order-N materials simulation. J Phys: Condens Matter, 2002, 14, 2745
[21] Monkhorst H J, Pack J D. Special points for Brillouin-zone integrations. Phys Rev B, 1976, 13, 5188
[22] Perdew J P, Burke K, Ernzerhof M. Generalized gradient approximation made simple. Phys Rev Lett, 1996, 77, 3865
[23] Zhuang H L, Singh A K, Hennig R G. Computational discovery of single-layer III-V materials. Phys Rev B, 2013, 87, 165415
[24] Fan X F, Zheng W T, Kuo J L, et al. Structural stability of single-layer MoS_2 under large strain. J Phys: Condens Matter, 2015, 27, 105401
[25] Lin S S. Light-emitting two-dimensional ultrathin silicon carbide. J Phys Chem C, 2012, 116, 3951
[26] Singh A K, Zhuang H L, Hennig R G. Ab initiosynthesis of single-layer III-V materials. Phys Rev B, 2014, 89, 245431
[27] Schwierz F. Graphene transistors. Nat Nanotechnol, 2010, 5, 487
[28] Riffe D M. Temperature dependence of silicon carrier effective masses with application to femtosecond reflectivity measurements. J Opt Soc Am B, 2002, 19, 1092
[29] Yadav D, Nair D R. Impact of source to drain tunneling on the ballistic performance of Si, Ge, GaSb, and GeSn nanowire p-MOS-

FETs. IEEE J Electron Devices Soc, 2020, 8, 308
[30] Quhe R G, Peng X Y, Pan Y Y, et al. Can a black phosphorus Schottky barrier transistor be good enough. ACS Appl Mater Interfaces, 2017, 9, 3959
[31] Sun X T, Xu L, Zhang Y, et al. Performance limit of monolayer WSe_2 transistors; significantly outperform their MoS_2 counterpart. ACS Appl Mater Interfaces, 2020, 12, 20633
[32] Yu B, Chang L, Ahmed S, et al. FinFET scaling to 10 nm gate length. IEEE International Electron Devices Meeting, 2002, 251
[33] Ni Z Y, Ye M, Ma J H, et al. Performance upper limit of sub-10 nm monolayer MoS_2 transistors. Adv Electron Mater, 2016, 2, 1600191
[34] Bennett B R, Ancona M G, Boos J B, et al. Strained GaSb/AlAsSb quantum wells for p-channel field-effect transistors. J Cryst Growth, 2008, 311, 47
[35] Bennett B R, Chick T F, Ancona M G, et al. Enhanced hole mobility and density in GaSb quantum wells. Solid State Electron, 2013, 79, 274
[36] Chen Y W, Tan Z, Zhao L F, et al. Mobility enhancement of strained GaSb p-channel metal –oxide –semiconductor field-effect transistors with biaxial compressive strain. Chin Phys B, 2016, 25, 038504
[37] del Alamo J A. Nanometre-scale electronics with III-V compound semiconductors. Nature, 2011, 479, 317
[38] Bansal A, Paul B C, Roy K. Modeling and optimization of fringe capacitance of nanoscale DGMOS devices. IEEE Trans Electron Devices, 2005, 52, 256
[39] Lacord J, Ghibaudo G, Boeuf F. Comprehensive and accurate parasitic capacitance models for two- and three-dimensional CMOS device structures. IEEE Trans Electron Devices, 2012, 59, 1332
[40] Wei L, Boeuf F, Skotnicki T, et al. Parasitic capacitances: Analytical models and impact on circuit-level performance. IEEE Trans Electron Devices, 2011, 58, 1361
[41] Vicarelli L, Vitiello M S, Coquillat D, et al. Graphene field-effect transistors as room-temperature terahertz detectors. Nat Mater, 2012, 11, 865
[42] Singh S, Thakar K, Kaushik N, et al. Performance projections for two-dimensional materials in radio-frequency applications. Phys Rev Appl, 2018, 10, 014022
[43] Prasanna Kumar S, Sandeep P, Choudhary S. Changes in transconductance (g_m) and I_{on}/I_{off} with high-K dielectrics in MX_2 monolayer 10 nm channel double gate n-MOSFET. Superlattices Microstruct, 2017, 111, 642

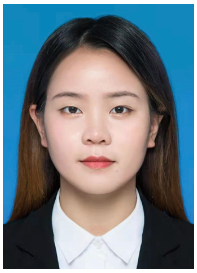

Panpan Wang was born in Inner Mongolia, China, 2000. Now she is an undergraduate of Beijing University of Posts and Telecommunications, majoring in applied physics. Her research focuses on the quantum transport simulations of sub-10 nm transistors.

Ruge Quhe got her PhD from Peking University. She is currently an Associate Professor with the School of Science, Beijing University of Posts and Telecommunications. Her research focuses on low-dimensional materials and electronics.